공학박사 학위논문

A study on the gelation dynamics of alginate gel and their application for gamma ray shielding

알지네이트 젤의 젤레이션 다이나믹스와 감마선 차폐로의 응용에 관한 연구

2020 년 2 월

서울대학교 대학원

재료공학부

권 석 현

A study on the gelation dynamics of alginate gel and their application for gamma ray shielding

알지네이트 젤의 젤레이션 다이나믹스와 감마선 차폐로의 응용에 관한 연구

지도 교수 오 규 환

이 논문을 공학박사 학위논문으로 제출함
2020년 2월

서울대학교 대학원
재료공학부
권 석 현

권석현의 공학박사 학위논문을 인준함
2019년 12월

위 원 장 안 철 희 (인)

부위원장 오 규 환 (인)

위 원 선 정 윤 (인)

위 원 강 석 훈 (인)

위 원 최 수 석 (인)

Abstract

A study on the gelation dynamics of alginate gel and their application for gamma ray shielding

Seok Hyeon Gwon

Department of Materials Science and Engineering

The Graduate School

Seoul National University

Alginates can be crosslinked with multivalent cations, leading eventually to hydrogel formation. The properties of alginate gel depend on its lock structure, monomeric composition, concentration of polymer and cross linker. Among these, the properties of ionically crosslinked alginate gel can be greatly affected by multivalent cations included as a cross linker. Knowledge of gelation dynamics by multivalent cations allows control over gelation characteristics, such as modulus of gel and the time required for equilibrium state, and healing properties. We have studied gelation dynamics of ionically crosslinked alginate gel. According to different types of anions bound with cations, gelation time and equilibrium viscosity was changed due to the solubility kinetics of the cation. The equilibrium viscosity is increased as period of the cations increased even though cations have same valency. A theoretical model is introduced to interpret dynamic change of viscosity during gelation.

In the next part, soft shields for gamma radiation were explored. Soft shields are required to protect the human body during a radioactive accident. However, the modulus of most soft shields, such as HDPE and epoxy, is high,

thereby making it difficult to process them in wearable forms like gloves and clothes. We synthesized a soft shield based on a hydrogel that is very compliant, stretchable, and biocompatible. The shields were fabricated by integrating γ-ray-shield particles into hydrogels with an interpenetrating network. The soft shields containing 3.33 M of PbO_2 exhibited a high attenuation coefficient (0.284 cm^{-1}) and were stretched to 400 % without a rupture. Furthermore, the fabricated soft shield can be sewn without a fabric support due to its high energy-dispersion ability. A wearable arm shield for the γ-ray radiation was demonstrated using a direct sewing of the soft-shield materials.

Keywords : Alginate, Gelation dynamics, Soft shield, γ-ray attenuation, Wearable shield

Student Number : 2011-20619

Table of Contents

List of Tables

List of Figures

Chapter 1. Introduction

1.1. Study background

1.1.1. Hydrogel

Hydrogels are polymer networks swollen with water. hydrogels are networks of polymer chains that are sometimes found as colloidal gels in which water is the dispersion medium.[1]

Researchers, over the years, have defined hydrogels in many different ways. The most common of defining ways is that hydrogel is a cross-linked polymeric network produced by one or more monomers and their solvent is water. Another definition is that it is a polymeric material that exhibits the ability to swell and retain a significant fraction of water within its structure, but will not dissolve in water. Hydrogels have received considerable attention in the past decades, due to their exceptional wide range of applications.[2-4] They possess also a degree of flexibility very similar to natural tissue due to their large water content.

The ability of hydrogels to absorb water arises from hydrophilic functional groups attached to the polymeric backbone, while their resistance to

dissolution arises from cross-links between network chains. Many materials, both naturally occurring and synthetic, fit the definition of hydrogels.

Recently, hydrogels have been defined as two- or multi-component systems consisting of a three-dimensional network of polymer chains and water that fills the space between macromolecules. Depending on the properties of the polymer (polymers) used, as well as on the nature and density of the network joints, such structures in an equilibrium can contain various amounts of water; typically in the swollen state, the mass fraction of water in a hydrogel is much higher than the mass fraction of polymer. In practice, to achieve high degrees of swelling, it is common to use synthetic polymers that are water-soluble when in non-cross-linked form.[5]

Among them, the hydrogel with an interpenetrating network is composed of ionically and covalently crosslinked networks, which can be stretched to 20 times their initial length and have fracture energies of 9,000 J/m^2.[6] Furthermore, despite the presence of a notch in the hydrogels, it can be stretched to 17 times their initial length due to the dissipation of the concentrated energy through the double network.[6] Also, hydrogels can be used as a neutron-shielding material because they contain ~ 90 % water.

Figure 1.1. Basic concept of gel.

1.1.2. Gamma radiation

The radiation that is emitted from radioactive materials can be classified as either α, β, γ, or neutron radiation according to the energy and the form of the radiated waves or particles.[7] The α and β rays with low-energy levels are easily blocked by an aluminum plate, while the γ-ray with a high-energy level can effectively be shielded by metals such as iron (Fe), tungsten (W), and lead (Pb) that comprise high atomic numbers and densities.[8] They decrease the transmission rate of the γ-ray through an interaction between the orbital electrons and the γ-ray.[9] Gamma rays are a form of electromagnetic radiation, whereby gamma radiation kills microorganisms by destroying cellular nucleic acid.[10]

Gamma radiation

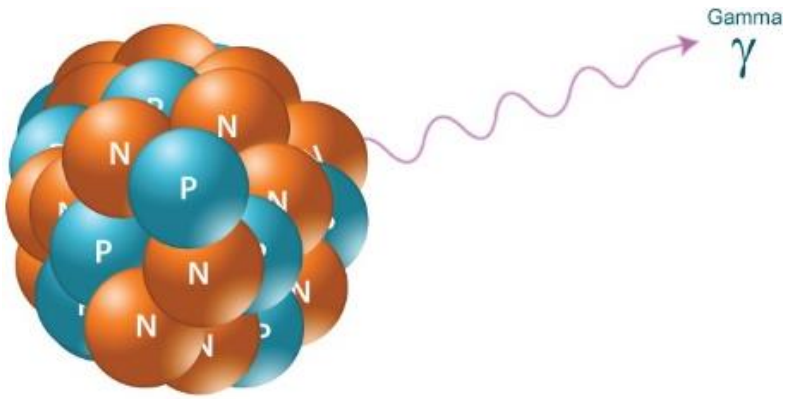

Figure 1.2. Gamma radiation : The emission of an high-energy wave from the nucleus of an atom

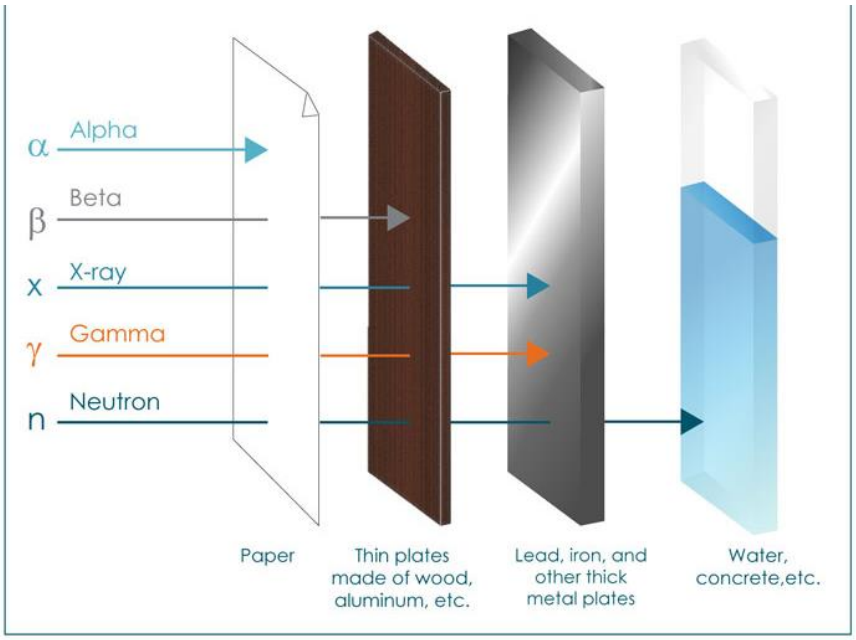

Figure 1.3. Types of radiation and penetration

1.2. The goal and outline of this thesis

This thesis studies the gelation dynamics of alginate gel and their application for gamma ray shielding. In chapter 2, gelation dynamics of ionically crosslinked alginate gel have been studied. A free growing model is applied to describe the gelation dynamics of ionically crosslinked alginate. Understanding of gelation dynamics enable to open up many applications for alginate gel limited by several weaknesses. Chapter 3, a sewable soft shield for radiation was synthesized through an integration of alginate/PAAm gels and metal oxides. Sewable soft shields with a shielding ability and a wearability are applicable in areas of the nuclear industry such as transportation, the storage of radioactive materials, and the protection of the human body following a radioactive accident. Conclusions and outlook of future research directions will be given at the end.

1.3. References

1. Enas M. Ahmed, Fatma S. Aggor, Ahmed M. Awad, Ahmed T. El-Aref, An innovative method for preparation of nanometal hydroxide superabsorbent hydrogel, Carbohydr Polym, 91 (2013), pp. 693-698
2. F.L. Buchholz, A.T. Graham, Modern superabsorbent polymer technology, Wiley- VCH, New York (1998)
3. L. Brannon-Peppas, R.S. Harland, Absorbent polymer technology, J Controlled Release, 17 (3) (1991), pp. 297-298
4. Yuhui Li, Guoyou Huang, Xiaohui Zhang, Baoqiang Li, Yongmei Chen, Tingli Lu, Tian Jian Lu, Feng Xu, Magnetic hydrogels and their potential biomedical applications, Adv Funct Mater, 23 (6) (2013), pp. 660-672
5. Enas M. Ahmed, Hydrogel: Preparation, characterization, and applications: A review, Journal of Advanced Research, Volume 6, Issue 2, 2015, pp. 105-121
6. Sun, J.-Y. et al. Highly stretchable and tough hydrogels. Nature 489, 133-136 (2012)
7. Siegbahn, K. Alpha-, beta-and gamma-ray spectroscopy. (Elsevier, 2012)
8. Bushberg, J. T. et al. Nuclear/radiological terrorism: emergency

department management of radiation casualties. The Journal of emergency medicine 32, 71-85 (2007)

9. Nelson, G. & Reilly, D. Gamma-ray interactions with matter. Passive Nondestructive Analysis of Nuclear Materials, Los Alamos National Laboratory, NUREG/CR-5550, LAUR-90-732, 27-42 (1991)

10. E.R.L. Gaughran, R.F. Morrissey, Sterilisation of Medical Products, Multiscience, New York (1980), vol. 2, 35–39

Chapter 2. Gelation dynamics of ionically crosslinked alginate gel

2.1. Introduction

Alginates are water-soluble biopolymers extracted from brown seaweed.[1, 2] Alginate is widely used as vehicles for cell delivery as well as wound dressing, dental impression, and immobilization matrix[3-5] due to its relatively low cost, biocompatibility, low toxicity, and simple gelation with various cations.[2, 5-7] However, many hydrogels as well as alginates tend to be brittle, and mechanical limitations exist.[8, 9] Most hydrogels have fracture energy as less than 100 J/m^2.[10] Because hydrogels are weak and brittle, it has been studied that hybrid hydrogels, consisting of interpenetrating networks (IPN) of two different polymers11. For example, alginate/polyacrylamide hydrogel has fracture energy as ~9000 J/m^2.[5] The alginate/PAAm hydrogel is also reported to biocompatible.[12] When a load is applied in alginate/PAAm hydrogel, ionically crosslinked alginates are unzipped and PAAm chains are stretched. The unzipping of the alginate network, increases the number of polymer chains which participate in loading and reduces the stress concentration.[5] Accordingly, it is possible to improve the toughness of

alginate gel as well as alginate/PAAm hydrogel by adjusting ionic crosslinking of the alginate.[13] The toughness of ionically crosslinked alginate can be adjusted by multivalent cations.[14] It is important to understand about gelation properties of alginate gel and enhance the mechanical property by adjusting ionically crosslinked alginate gel. It can open up many applications for hydrogels limited by poor mechanical properties of hydrogels.

Ionic crosslinking of alginate are formed by the binding of multivalent cations between guluronic acid (G-blocks) on different alginate chains (Figure 2.1. (a)).[15] The typical model depicting the ionic crosslinking between alginate and the cation is the egg-box model (Figure 2.1. (b)).[15-17] Divalent cations such as calcium bind preferentially to the G-blocks in the alginate in a highly cooperative manner.[14, 18, 19] As a result, an alginate gel can have a wide range of gel strengths. In many applications, the gelation behavior of hydrogels plays significant roles. This paper focuses on the gelation forming behavior of alginates.

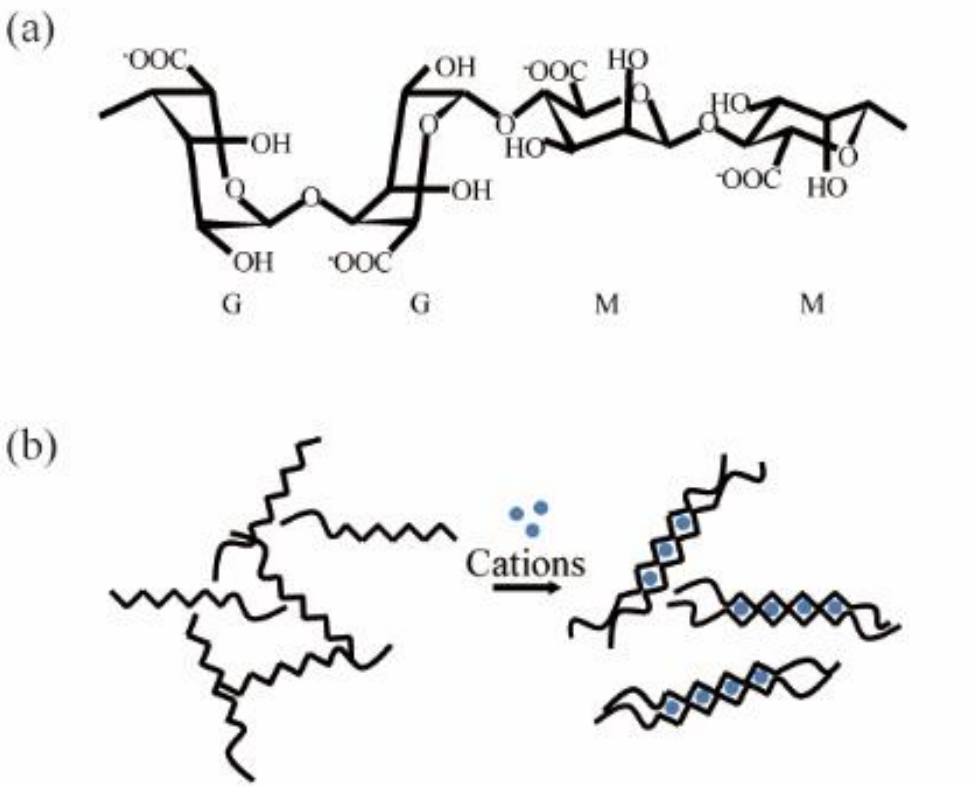

Figure 2.1. Ionic crosslinking of alginate-gel (a) Alginate polymers are consisted with G(Guluronic acid) and M(Mannuronic acid) blocks. (b) G blocks of alginate can be crosslinked with various cations.

2.2. Experimental section

2.2.1. Gel fabrication

6 g of sodium alginate (Protanal LF 200S, FMC) were dissolved in deionized water (194 ml), and stored at 4℃ for 3days to obtain a homogeneous and transparent 3% alginate solution. Then, 0.16M of cross linker solutions (LiCl, NaCl, $CaSO_4$, $CaCl_2$, $SrSO_4$, $SrCl_2$, $BaSO_4$, $BaCl_2$, $MgSO_4$, and $MgCl_2$) were mixed with alginate solution to examine the formation of crosslinking. The number of cation in the gels was adjusted to be equal when these salts are completely dissociated.

2.2.2. Viscosity measurement

Viscosity of the alginate gel was measured with SV-10 viscometer (A & D Company). Schematics for viscosity measurement are shown in Figure 2.2. To prevent water evaporation of alginate solution, it was covered by several millimeters of oil.

In the viscometer model used in this experiment, mechanical impedance is represented as follows.[20]

$$A\sqrt{\pi f \eta \rho} = \frac{F}{Ve^{i\omega t}} \quad (1)$$

Where A is a planar dimension of two oscillators, f is a vibration frequency, η is a fluid viscosity, ρ is a fluid density, F is a force induced by electromagnetic drive unit and $Ve^{i\omega t}$ is a oscillators' constant vibration velocity.

Using equation (1), the interaction formula between the electromagnetic force F exerted from the instrument and viscosity η is established. Remaining constant values can be evaluated in routine methods, and the force F is a function of electric current and thus viscosity is measured at every moment in a simple way. The measuring range of viscosity was 0.3 – 12,000 mPa·s.

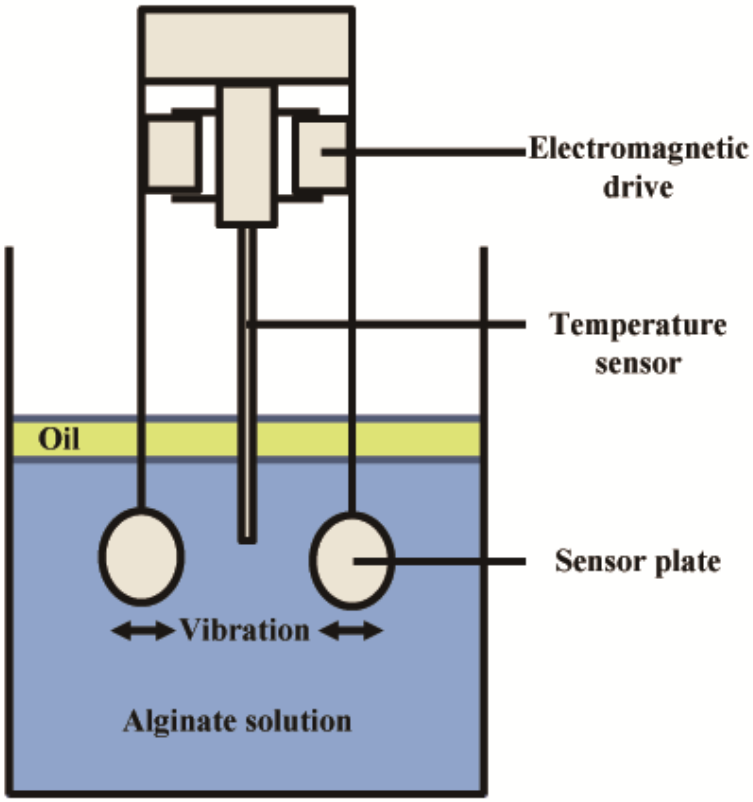

Figure 2.2. Schematics of viscosity measurement system for ionically crosslinked alginate gel.

2.3. Results and Discussion

2.3.1. Gelation of the ionically crosslinked alginate gel

Figure 2.3 shows gelation speeds of ionically crosslinked alginate gel with various cations. As shown in Figure 2.3. (a), change of viscosity in alginate solution is small when monovalent cations were used as a cross linker. Coulomb attraction between the cations and the oppositely charged alginate chains in the solution must give an excess of attractive force which exceed the repulsive force of anions to stabilize the binding of the chains. However, as monovalent cations form an ionic binding with alginate chains, Coulombic force of the monovalent cation is not sufficient comparing with repulsive force of anion (COO^-), so that the monovalent cations could not crosslink the alginate chains. On the other hand, a viscosity of alginate solution mixed with divalent cations increases as gelation time increases, indicating that divalent cations crosslink the alginate chains successfully. (shown in Figure 2.3. (b))

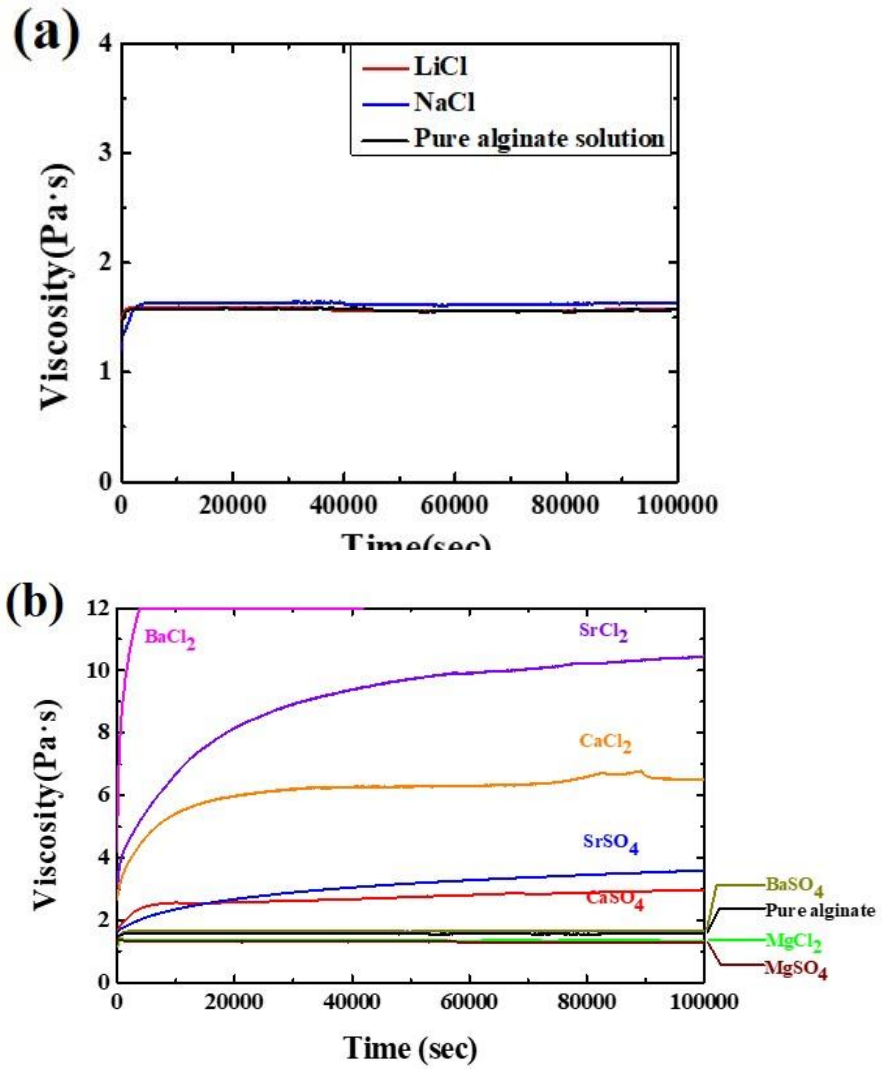

Figure 2.3. (a) Viscosity change of the alginate solution with monovalent cations. (b) Viscosity change of the alginate solution with divalent cations.

2.3.2. Gelation mechanism : a free growing model

In order to extract gelation parameters (i.e. gelation time and final viscosity of alginate gel) from our experimental results, we will now outline a simple gelation mechanism. For the gelation process, growth of nuclei from each cluster should be considered, described by a free growing model as shown in Figure 2.4. A free growing model for gel cluster include the law of mass conservation and one assumption; the cluster formed by spherical growth of nuclei. Since a spherical shape can minimize the surface energy, the assumption of spherical growth of nuclei is appropriate.[21]

In spherical cluster growth, the relation between the volume of gel cluster *V* and radius of gel cluster at specific time *r* is:[22, 23]

$$dV : V = 4\pi r^2 dr : \frac{4\pi r^3}{3} \tag{2}$$

$$\frac{dV}{dx} = \frac{3V}{x} \tag{3}$$

where *x* is the relative variable ($x = \frac{r}{r_\infty}$) and r_∞ is the radius of gel cluster at equilibrium. For non-spherical geometry, equation (3) can be modified by:[24]

$$\frac{dV}{dx} = \frac{nV}{x} \tag{4}$$

By integrating equation (4), equation (5) is obtained.

$$V = V_{\infty} x^{n} \tag{5}$$

where V_{∞} is the volume of cluster at equilibrium, n is the proportionality constant.

The infinitesimal change of x with time t is given in equation (6).

$$\frac{dx}{dt} = \frac{dx}{dr}\frac{dr}{dV}\frac{dV}{dt} \tag{6}$$

$$\frac{dx}{dr} = \frac{1}{r_{\infty}} \tag{7}$$

$$\frac{dr}{dV} = \frac{1}{4\pi r^{2}} = \frac{1}{4\pi x^{2} r_{\infty}^{2}} \tag{8}$$

Equation (7) and (8) were derived from definition of x, r, r_{∞} and V. In order to derive $\frac{dV}{dt}$, we assumed that the concentration change of the alginate gel is proportional to the concentration of the gel which was excluded to form a cluster in the solution. Since alginate has long chain morphology, mobility of alginate chain decreases as more gel clusters are formed. On the other hand, comparatively small chain can move freely in solution until they bind with other alginates. For this reason, alginate concentration in solution plays a critical role

in the reaction rate. As a result, equation (9) is obtained.

$$\frac{dV}{dt} = k\left(\frac{4\pi r_{\infty}^3}{3} - \frac{4\pi r^3}{3}\right) = k\left(\frac{4\pi r_{\infty}^3}{3} - \frac{4\pi r_{\infty}^3 x^3}{3}\right) \quad (9)$$

where *k* is the velocity constant. From equation (6), (7), (8), and (9), equation (10) is obtained.

$$\frac{dx}{dt} = \frac{k(1-x^3)}{3x^2} \quad (10)$$

Since nuclei have certain amount of radius at the beginning of the nucleation, equation (10) is always valid ($x \neq 0$). After integrating equation (10), an expression for *x* on *t* can be obtained. As time converge to zero($t \rightarrow 0$), x value also converge to zero($x \rightarrow 0$), and at equilibrium, $t=\infty$, $x=1$ shown in equation (11).

$$x^3 = 1 - C' exp(-kt) \quad (11)$$

where C' is the integration constant($C<1$). Finally, from equation (5) and equation (11), the volume of one gel cluster as a function of time is:

$$V = V_{\infty}[1 - \exp(-Ct)]^{n/3} \quad (12)$$

where C is the constant derived by multiplication k with natural logarithm C'. Meanwhile, viscosity of α and β phases(η_a and η_b respectively), can be expressed as:[25]

$$\frac{1}{\eta_{total}} = \frac{\chi_a}{\eta_a} + \frac{\chi_b}{\eta_b} \quad (13)$$

where χ_a is the mol fraction of the gel phase, χ_b the mol fraction of the solution-phase. By assuming that the volume change of sol-gel transition is very small, mol fraction can be expressed as volume fraction.

$$\chi_a = \frac{NV}{V_t}, \ \chi_b = \frac{(V_t - NV)}{V_t} \quad (14)$$

$$\eta_{total} = \frac{1}{\frac{NV}{V_t\eta_a} + \frac{(V_t - NV)}{V_t\eta_b}} = \frac{1}{\frac{1}{\eta_b} + \frac{NV}{V_t}\left(\frac{1}{\eta_a} - \frac{1}{\eta_b}\right)} \quad (15)$$

$$\frac{NV}{V_t}\left(\frac{1}{\eta_a} - \frac{1}{\eta_b}\right) = \frac{NV_{\infty}\{1-\exp(-Ct)\}^{n/3}}{V_t}\left(\frac{1}{\eta_a} - \frac{1}{\eta_b}\right) = M\{1 - \exp(-Ct)\}^{n/3} \quad (16)$$

$$\eta_{total} = \frac{1}{\frac{1}{\eta_b} + M\{1-\exp(-Ct)\}^{n/3}} \quad (17)$$

where η_b indicates the initial viscosity before crosslinking. *N* is the number of nuclei, V_t is the total volume of solution, and *M* is grouping constant.

By using equation (17), the fitting viscosity curve can be obtained as shown in Figure 2.5 and Table 2.1. A coefficient of determination, R-squared for each fitting curve has a value close to 1, indicating that the fitting curve is reasonable. On the other hand, for $BaSO_4$ and pure alginate, they could not form an ionic crosslinking, so the coefficient of determination value is less close to 1.

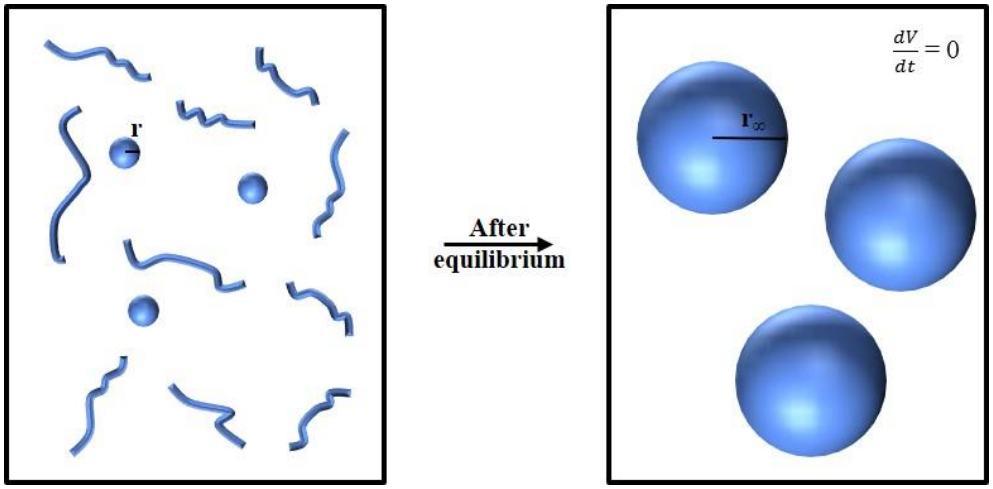

Figure 2.4. A free growing model for a gel cluster during gelation process. The volume change of gel cluster over time (dV/dt) is zero at equilibrium state.

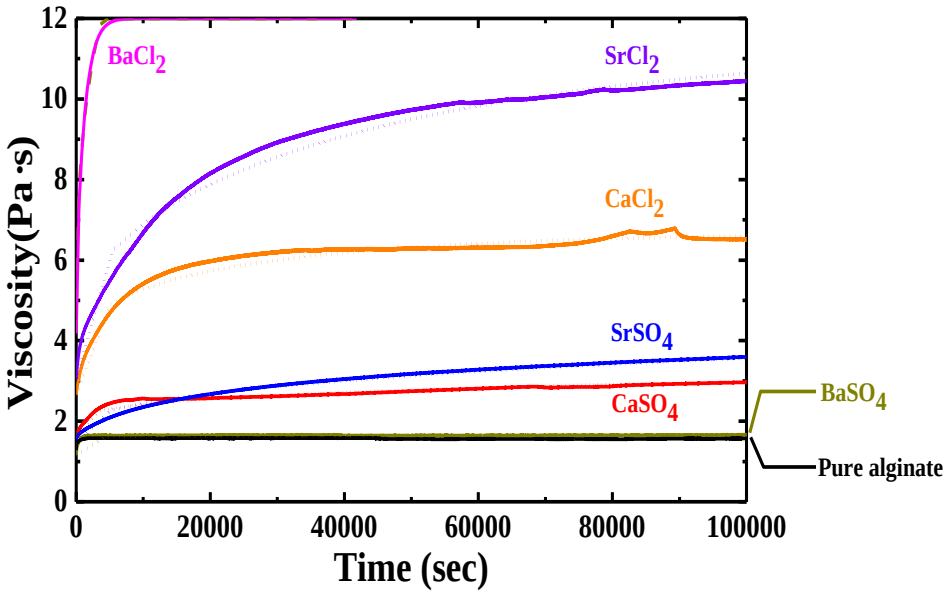

Figure 2.5. Viscosity change of alginate solution obtained by experiment (solid line), and free growing model. (dotted line)

Cross linker	η_b(Pa·s)	M (Pa·s^{-1})	C (1/s)	n	Coefficient of determination	Solubility
$CaCl_2$	2.652	-0.228	2.68 x 10^{-5}	0.133	0.654	81.1 g/100 mL (25 °C)
$CaSO_4$	1.596	-0.356	2.79 x 10^{-6}	0.145	0.968	0.24 g/100ml at 20 °C
$SrCl_2$	3.073	-0.237	1.96 x 10^{-5}	0.157	0.962	53.8 g/100 mL (20 °C)
$SrSO_4$	1.439	-0.472	6.80 x 10^{-6}	0.184	0.984	0.0135 g/100 mL (25 °C)
$BaCl_2$	4.184	-0.156	8.37 x 10^{-4}	0.336	0.988	35.8 g/100 mL (20 °C)
$BaSO_4$	1.162	-0.365	7.87 x 10^{-11}	0.028	0.472	0.0002448 g/100 mL (20 °C)

Table 2.1. The parameters of free growing model which were obtained from fitting curves in (Figure 2.5). Initial viscosity (η_b) and the other values (M, C, n) were calculated by equation (17).

2.3.3. Gelation results of ionically crosslinked alginate gel

The equilibrium value of viscosity can be calculated from equation (17) ($t=\infty$). In addition, the time required for viscosity to reach 95% and 99% of equilibrium also can be calculated, as shown in Table 2.2. In case of $BaSO_4$, $MgCl_2$, $MgSO_4$, and pure alginate, crosslinking was not successful, so that only the equilibrium viscosity is described. Although same cation is used, if they bound with different anions, different effect resulted. Chlorides have large equilibrium viscosity whereas sulfates have lower equilibrium viscosity. When calcium and strontium salts are used as cross linker, equilibrium viscosity and 95% gelation time are shown in Figure 2.6. (a) and (b). As shown in Figure 2.6. (a), with the increase of period where the cation is belonging, equilibrium viscosity also increased even though electrostatic force is same. From Figure 2.6. (a), the other factor can be said to be cation size. When cation size is too small, comparable to Mg^{2+}, alginate chain binding is unstable because of repulsive force between the two alginate chains in the egg-box model. Meanwhile, when period number of cation increases, the ionic radius also increases; can stabilizing the bonding between the two alginate chains. Increase of the distance between the two chains decreases an electrostatic repulsion force between the COO^- functional group, and can stabilize the ionic crosslinking.

As shown in Figure 2.6. (b), sulfate salts showed longer gelation time compared to chloride salts, since the solubility of sulfate salts is lower than that

of chloride salts, which attribute to low degree of electrolytic dissociation of sulfate slowing down supply of cations. In order to analyze gelation time, the solubility and binding efficiency of each ion should be considered. Moreover, according to Pauling scale, Ca, Sr, and Ba showed electronegativities of 1, 0.95, and 0.89, respectively. It is predicted that lower electronegativity of Ba allows the bonding with alginate to become more ionic and is expected to have higher binding efficiency. The reason for fast binding of Ba^{2+} in chloride salts with alginate chain can be attributed to appropriate size effects and large solubility with low electronegativity. Higher solubility leads to higher rate of gelation because of faster cation supply.

Cross linker	95% gelation time(10^3 sec)	99% gelation time(10^3 sec)	Equilibrium viscosity(Pa·s)
$MgCl_2$	-	-	1.308
$MgSO_4$	-	-	1.253
$CaCl_2$	54.60	112.84	6.708
$CaSO_4$	503.57	1061.33	3.696
$SrCl_2$	108.75	190.80	11.310
$SrSO_4$	302.47	538.68	4.486
$BaCl_2$	3.00	4.95	12.047
$BaSO_4$	-	-	2.018

Table 2.2. An estimated time and viscosity corresponding 95%, 99% of the equilibrium viscosity after the time has flown enough.

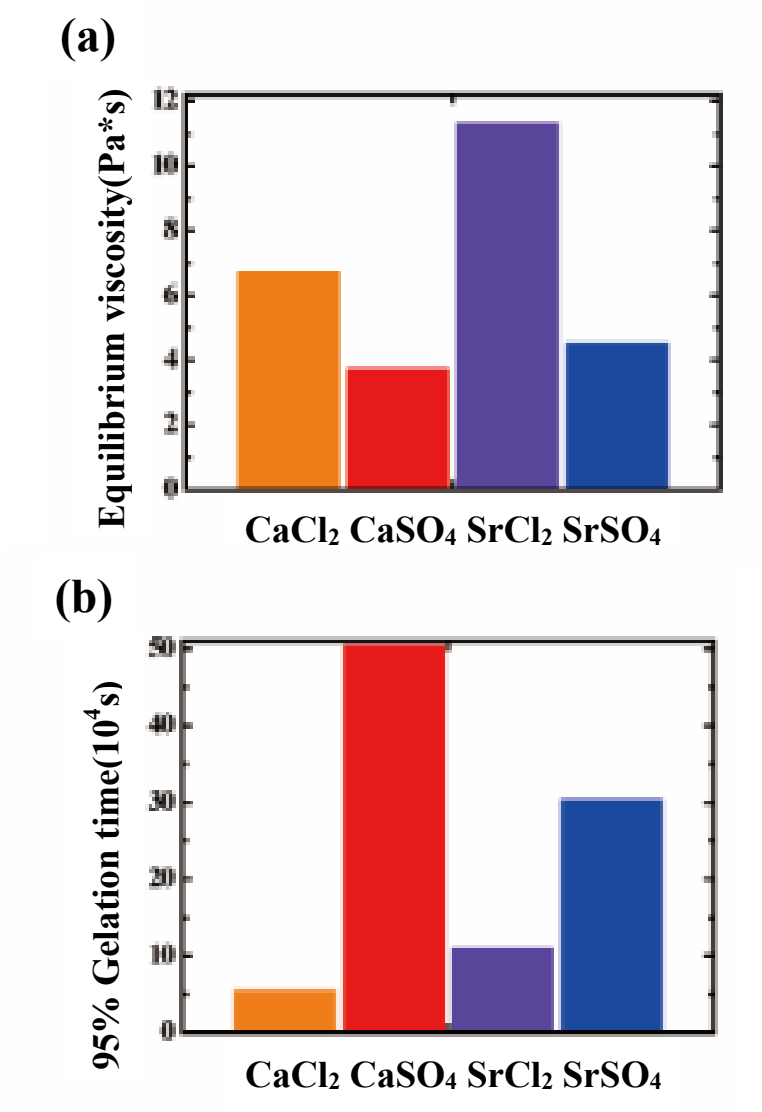

Figure 2.6. Key values of gelation calculated from free growing model for calcium and strontium salts (a) Equilibrium viscosity (b) 95% gelation time.

2.4. Conclusion

Gelation dynamics of ionically crosslinked alginate gel have been studied. A free growing model is applied to describe the gelation dynamics of ionically crosslinked alginate. As a result, using a specific function, we could figure out a general formula for describing cross linker in which ionic crosslinking occurred. As period number of cation increases, lager cation can stabilize the bonding between the two alginate chains. In gelation time, the solubility and binding efficiency of salts are considered. Usually, solubility of cross linker salts effects on gelation time since it is directly associated with supply of cross linker cations. Understanding of gelation dynamics enable to open up many applications for hydrogels as well as alginate gel limited by several weaknesses. As research and development continues with ionically crosslinked alginate, we expect to see many innovative and exciting applications for biological hydrogel material in the future.

2.5. References

1. L. Shapiro and S. Cohen, *Biomaterials.*, **18**, 583 (1997).
2. O. Smidsrød, *Trends Biotechnol.*, **8**, 71 (1990).
3. W.R. Gombotz and S.F. Wee, *Adv. Drug Delivery Rev.*, **64**, 194 (2012).
4. G. Klöck, A. Pfeffermann, C.Ryser, P. Gröhn, B. Kuttler, H. Hahn, U. Zimmermann, *Biomaterials*, **18**, 707 (1997).
5. J.Y. Sun, X. Zhao, W. R. Illeperuma, O. Chaudhuri, K.H. Oh, D.J. Mooney, J.J. Vlassak, Z. Suo, *Nature*, **489**, 133 (2012).
6. J.L. Drury and D.J. Mooney, *Biomaterials*, **24**, 4337 (2003).
7. Y. Qiu and K. Park, *Adv. Drug Delivery Rev.*, **53**, 321 (2001).
8. P. Calvert, *Adv. Mater.*, **21**, 743 (2009).
9. D.J. Huey, J.C. Hu, and K.A. Athanasiou, *Science*, **338**, 917 (2012).
10. G. Lake and A. Thomas, *Proc. R. Soc. London, A.*, **300**, 108 (1967).
11. J.P. Gong, Y. Katsuyama, T. Kurokawa, Y. Osada, *Adv. Mater.*, **15**, 1155 (2003).
12. M.C. Darnell, J.Y. Sun, M. Mehta, C. Johnson, P.R. Arany, Z. Suo, D.J. Mooney, *Biomaterials*, **34**, 8042 (2013).
13. C.H. Yang, M.X. Wang, H. Haider, J.H. Yang, J.Y. Sun, Y.M. Chen, J. Zhou, Z. Suo, *ACS Appl. Mater. Inter.*, **5**, 10418 (2013).
14. Ý.A. Mørch, I. Donati, B.L. Strand, G. Skjåk-Bræk,

Biomacromolecules, **7**, 1471 (2006).

15. T. Bryce, A. McKinnon, E. Morris, D. Rees, D. Thom, *Faraday Discuss. Chem. Soc.*, **57**, 221 (1974).
16. I. Braccini and S. Pérez, *Biomacromolecules*, **2**, 1089 (2001).
17. G.T. Grant, E.R. Morris, D.A. Rees, P. Smith, D. Thom, *FEBS Lett.*, **32**, 195 (1973).
18. A. Haug and O. Smidsrod, *Acta Chem. Scand*, **19** (1965).
19. A. Haug and O. Smidsrod, *Acta Chem. Scand*, **24**, 843 (1970).
20. N. IZUMO and A. KOIWAI, in *Proceedings of Asia-Pacific Symposium on Measurement of Mass, Force and Torque (APMF 2009)*2009, pp 1-4.
21. R. Van Keer and J. Kacur, *Math. Probl. Eng.,* **4***,* 115 (1998).
22. A. Blandino, M. Macias, and D. Cantero, *J. Biosci. Bioeng.*, **88**, 686 (1999).
23. J. Chrastil, *J. Agric. Food Chem.*, **39**, 874 (1991).
24. J. Chrastil, *Int. J. Biochem.*, **20**, 683 (1988).
25. M. Awad and Y. Muzychka, *Exp. Therm. Fluid. Sci*., **33**, 106 (2018).

Chapter 3. Sewable soft shields for the γ-ray radiation

3.1. Introduction

In 2011, the Fukushima Daiichi nuclear disaster occurred due to the Great East Japan Earthquake and tsunami. Radioactive isotopes were released from reactor-containment vessels, and the Japanese government implemented an exclusion zone around the power plant.[1] The World Health Organization (WHO) released a report that predicted an increase of the risk regarding specific health effects for the populations living around the Fukushima nuclear-power plant.[2] Accordingly, the anxiety about radiation leaks and the interest in radiation shields increased.

The radiation that is emitted from radioactive materials can be classified as either α, β, γ, or neutron radiation according to the energy and the form of the radiated waves or particles.[3] The α and β rays with low-energy levels are easily blocked by an aluminum plate, while the γ-ray with a high-energy level can effectively be shielded by metals such as iron (Fe), tungsten (W), and lead (Pb) that comprise high atomic numbers and densities.[4] They decrease the transmission rate of the γ-ray through an interaction between the

orbital electrons and the γ-ray.[5] Concrete compounds are generally used to shield the γ-ray, but because they are bulky and heavy, metal-concrete composites are used only for nonmobile structures (i.e., buildings).[6-8] Polymer-matrix metal composites such as high-density polyethylene (HDPE) or epoxy composited with high-density metal particles have recently garnered attention as a γ-ray shield material.[9, 10] These polymers are less efficient for shielding the γ-ray but are relatively light compared to metals and concrete compounds. However, HDPE and epoxy are naturally stiff, making them difficult to process for clothing manufacturing because of their high modulus.[11, 12]

Hydrogels are very compliant materials that, like the human skin, have a Young's-modulus range from 10 kPa to 10 MPa.[13-16] However, hydrogels are rarely used for structural materials because most hydrogels are brittle.[17, 18] Therefore, researchers have struggled to develop a mechanically tough hydrogel with the use of many strategies such as interpenetrating networks and nanocomposites.[19-21] Among them, the hydrogel with an interpenetrating network is composed of ionically and covalently crosslinked networks, which can be stretched to 20 times their initial length and have fracture energies of 9,000 J/m^2. [22] Furthermore, despite the presence of a notch in the hydrogels, it can be stretched to 17 times their initial length due to the dissipation of the

concentrated energy through the double network.[22] Also, hydrogels can be used as a neutron-shielding material because they contain ~ 90 % water.

In this study, a wearable soft shield was fabricated from hydrogels that had been integrated with shield particles. To improve the wearability of the soft shield, the focus was the mechanical properties of the soft shield, especially the sewability.

3.2. Experimental section

3.2.1. Gel fabrication

Here, the synthesis of a sewable soft shield for the γ-ray radiation was achieved through the integration of hydrogels and metal oxides, for which 1 g of sodium alginate and 8 g of acrylamide were dissolved in deionized water (86 wt% water contents) and stored at 4 ℃ for 3 days to obtain a homogeneous solution. N,N,N',N'-tetramethylethylenediamine and 0.1 M N,N-methylenebisacrylamide (MBAAm) were added as a crosslinking accelerator for the poly(acrylamide) and a crosslinker for the poly(acrylamide), respectively. A metal-oxide (Fe_2O_3, WO_3, and PbO_2) slurry was added into the alginate/acrylamide solution. Then, a solution comprising 0.2 M ammonium persulphate and 1.22 M calcium sulfate was added as a thermal initiator for the poly(acrylamide) and as an ionic crosslinker for the alginate. A uniformly distributed hydrogel solution was poured into a glass mold and cured with ultraviolet light (with 8 W of power and a 254-nm wavelength) for 1 hr before it was stabilized at room temperature for 2 days. The overall synthesis procedure of the soft shields is shown in Figure 3.1.

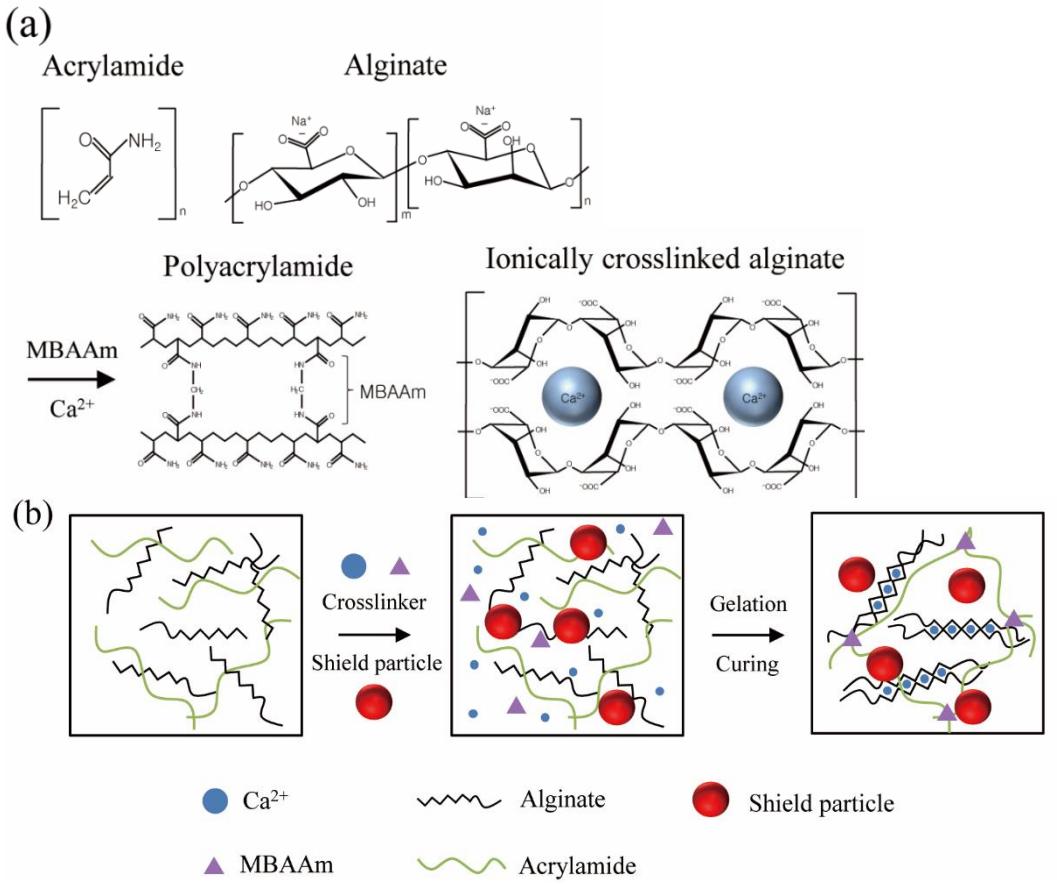

Figure 3.1. Synthesis procedures of soft shields for the γ-ray radiation. (a) Poly(acrylamide) was covalently crosslinked with N,N-methylenebisacrylamide (MBAAm), and alginate was ionically crosslinked with the Ca^{2+} cation. (b) The soft shield for the γ-ray radiation was synthesized by integrating the microshield particles into a highly stretchable and soft hydrogel matrix.

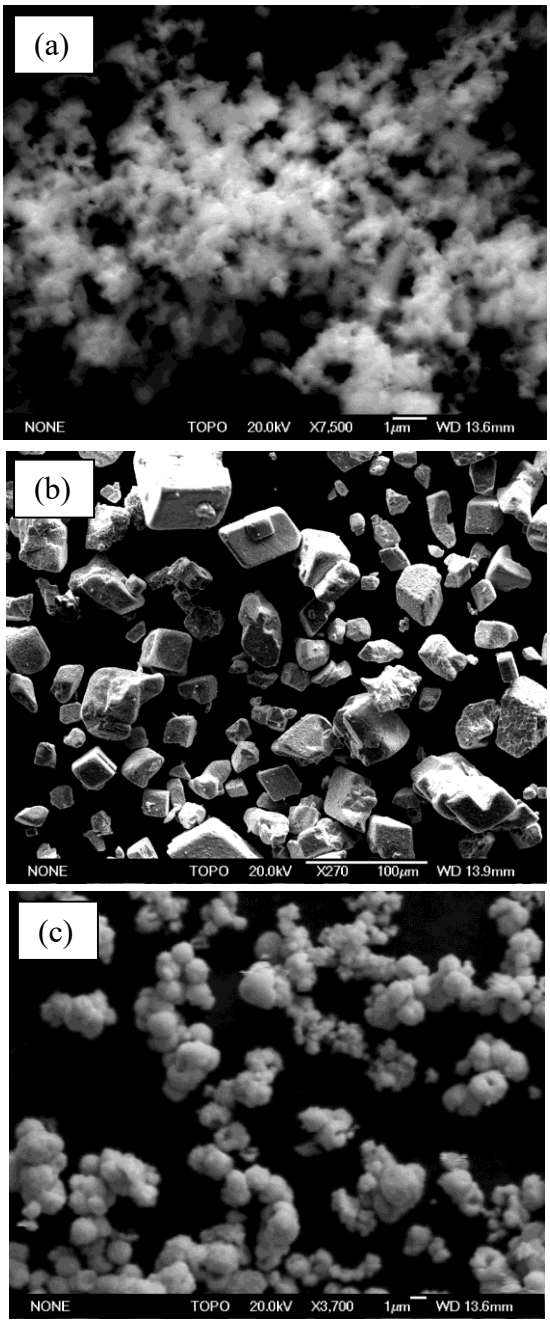

Figure 3.2. SEM images of shield particle (a) Fe_2O_3, (b) WO_3, (c) PbO_2

3.2.2. Measurement of the γ-ray transmission

To measure the transmission rate of the passing of the γ-ray through the shielding material, the device that is shown in Figure 3.3 was customized for the present study. The radiation-source stand was designed with the inner, vertical, and horizontal diameters of 5 mm, 40 mm, and 25 mm, respectively. A γ-ray path from the source was sealed with a lead-metal shield to prevent the radiation scattering toward the detector. The soft shield was placed between the detector and the radiation-source stand. Then, the transmission rate of the soft shields was measured using the previously mentioned device. The radiation source of Cs-137 (0.662 MeV) was manufactured in November 2011, and the activity is 5 μCi. Various soft shields with a thickness of 5 mm were used in the transmission-rate measurements. During the measurements, 800 V of voltage were applied to the detector three times for 600 s each time.

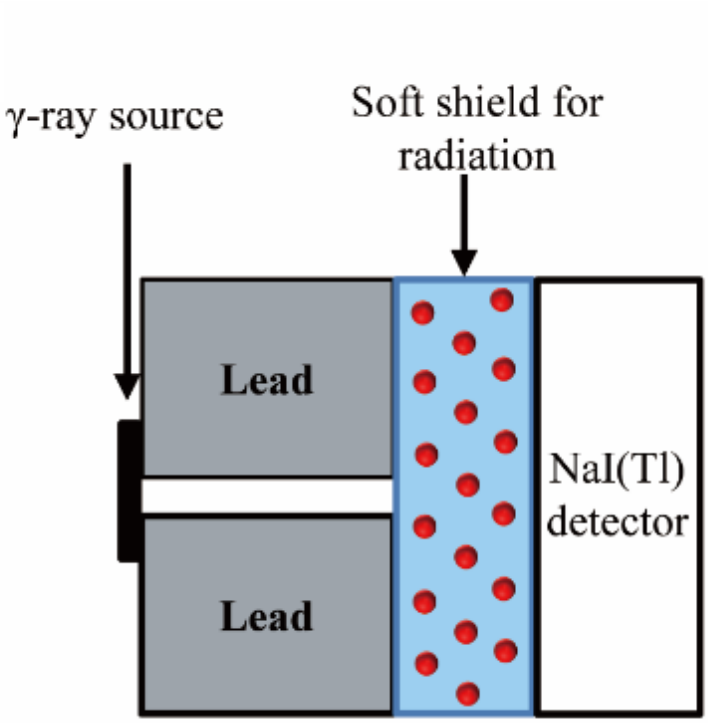

Figure 3.3. A schematic illustration for an experimental measurement of the γ-ray transmission with a Cs-137 (0.662 MeV) radiation source.

3.2.3. Mechanical test

A tensile test was performed at room temperature using the Instron 3343 tensile machine (Instron, U.S.A.) with a 50 N load cell to determine the mechanical properties of the soft shield for the γ-ray radiation. The specimen size was adjusted to 10.0 × 10.0 × 3 mm^3, as shown in Figures 3.4 (a) and 3.4 (b). Each soft shield was mounted on the tensile tester and then stretched until a mechanical rupturing occurred with a loading velocity of 6 mm/min.

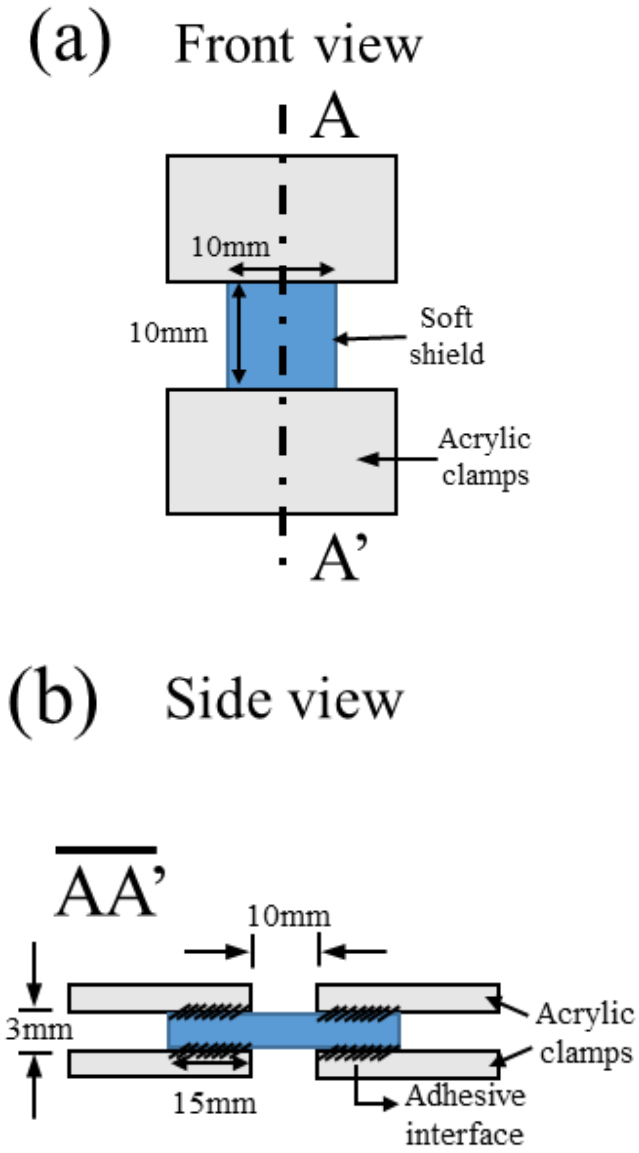

Figure 3.4. The geometry of tensile specimens.

3.3. Results and Discussion

3.3.1. The principle of the γ-ray attenuation

The principle of the soft-shield γ-ray attenuation is shown in Figure 3.5. The shielding of the γ-ray radiation was primarily induced by an interaction between the electrons in the shield particles and the γ-ray.[5, 23] The γ-ray interacted with an atom resulting in the ejection of an electron. The electron then received energy from the γ-ray, and this may induce the secondary ionization of the electron. During the passing of the γ-ray through the shielding material, the γ-ray intensity was decreased. To estimate the ability of the γ-ray shield, it is important to quantify the transmitted γ-ray. The transmission rate and the attenuation coefficient are shown by equation (1), as follows:

$$Transmission\ rate(T) = I/I_0 = e^{-\mu t}, \quad (1)$$

where I is the postshielding intensity, I_0 is the incident intensity, μ is an attenuation coefficient, and t is the shielding-material thickness.[24] The mass attenuation coefficient (μ_m) of the compound is shown by equation (2), as follows:

$$\mu_m = {}^{\mu}/_{\rho} = \sum_i w_i(\mu_m)_i \quad (2)$$

where ρ is the shield-material density, and w_i and $(\mu_m)_i$ are the weight fraction and the mass attenuation coefficient of the ith-constituent element, respectively. For the present work, metal oxides and hydrogel were used as the constituents.

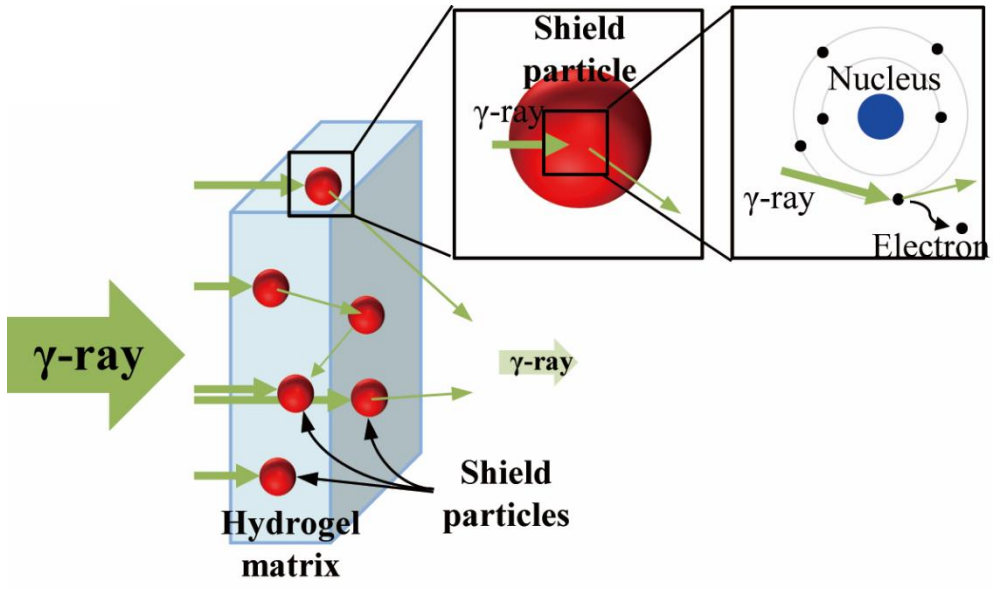

Figure 3.5. The γ-ray was attenuated by interactions between electrons and shield particles.

3.3.2. The attenuation coefficient of the soft shields

Figure 3.6 shows a logarithmic-scale plot of the γ-ray-transmission rates as a function of the soft-shield thickness. The shields contain 3.33 M of each shield particle. The γ-ray-transmission rate was decreased by an interaction between the orbital electrons of the metal oxide and the γ-ray. As shown in Figure 3.6 (a), the transmission rate was linearly decreased as the soft-shield thickness was increased. In addition, the transmission rate of the soft shields containing lead oxide (PbO_2) powder is much lower than that of the other soft shields containing tungsten trioxide (WO_3) and ferric oxide (Fe_2O_3) powders, suggesting that as the atomic number of the metal-oxide powder was increased, the interaction probability between the γ-ray and the electron was increased proportionally. Therefore, the soft shield including heavy elements such as PbO_2 powder is more effective than those containing WO_3 and Fe_2O_3 powders; accordingly, the soft shield including WO_3 powder is more effective than that including Fe_2O_3 powder.

To obtain the attenuation coefficients for the soft shields including the metal-oxide powders, a slope was fitted with a graph, as shown in Figure 3.6 (a). The attenuation coefficient of the soft shield for the Cs-137 γ-ray at 0.662 MeV was evaluated using equation (1). Figure 3.6 (b) shows the attenuation coefficients of the various soft shields. The attenuation coefficient of the pristine soft shield without any metal-oxide powder is 0.216 cm^{-1},

which is higher than that of the soft shield with metal aluminum (0.2 cm^{-1}).[25] This result is attributed to the high mass attenuation coefficient and the suitable molecular structure of the water for the γ-ray-radiation shielding. In the cases of the soft shields including iron, tungsten, and lead oxides, the attenuation coefficients are 0.229, 0.251, and 0.284 cm^{-1}, respectively. For the soft shields with a metal oxide containing a high atomic number, the attenuation coefficients of the soft shields were increased. Accordingly, the volume of the heavy-metal particles per unit volume is a primary factor of the radiation-shield ability. Pure metals (i.e., Fe, W, and Pb) will show more favorable attenuation abilities than metal oxides because they contain more metal atoms per unit volume. But metals are unstable in hydrogel because they will be gradually oxidized. Therefore, the investigation of the metal oxides is only regarding the stability of the shield.

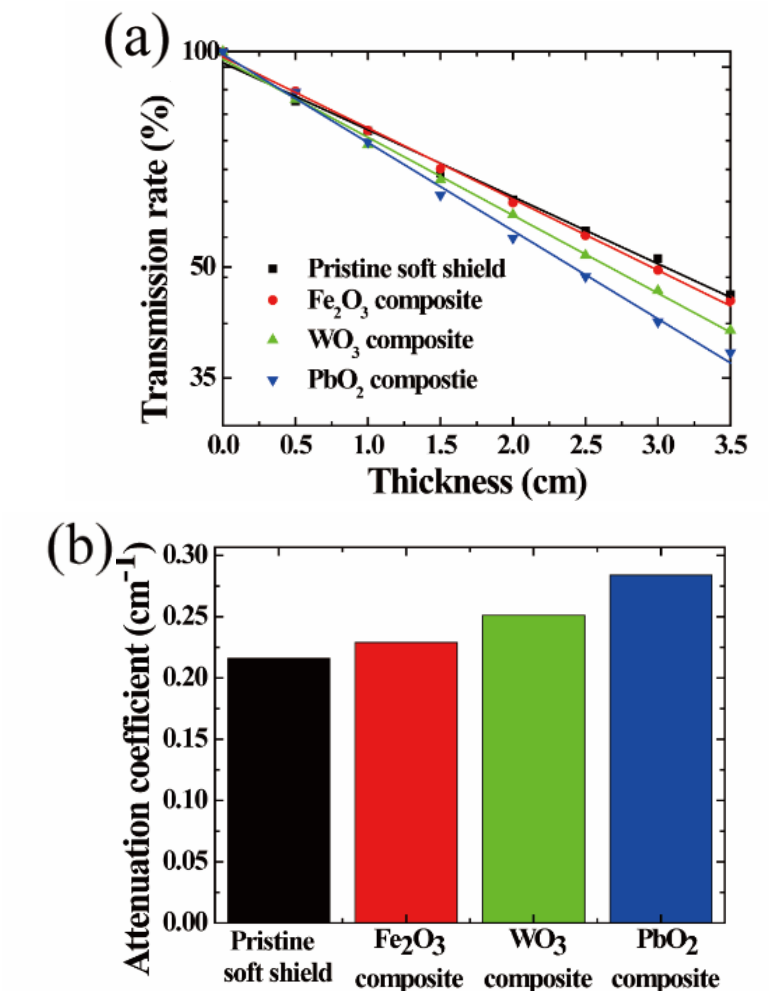

Figure 3.6. (a) The transmission rates for the γ-ray radiation were investigated using the thickness of the soft shields. The shields contain 3.33 M of each shield particle. (b) The attenuation coefficients of the soft shields were evaluated from the transmission rates.

3.3.3. Analytic calculations of the attenuation coefficient

Using equation (2), the attenuation coefficient for the added amount of lead oxide is shown in Figure 3.7.

$$\mu_{com} = \rho_{com}\left(\frac{x_M}{x_M+x_g} * \frac{\mu_M}{\rho_M} + \frac{x_g}{x_M+x_g} * \frac{\mu_g}{\rho_g}\right) \quad (3)$$

Where μ_{com} is the attenuation coefficient of composite, μ_M is the attenuation coefficient of metal oxide, μ_g is the attenuation coefficient of gel, ρ_{com} is the density of composite, ρ_M is the density of metal oxide and ρ_g is the density of gel.

Analytic calculations were made with values of hydrogel ($\rho_{hydrogel}$ = 1.13 g cm^{-3}, $\mu_{hydrogel}$ = 0.216 cm^{-1}) and bulk lead oxide (ρ_{PbO2} = 9.38 g cm^{-3}, μ_{PbO2} = 1.020 cm^{-1}). The density and attenuation-coefficient measurements of the hydrogel are presented in Figure 3.6 (b). The lead-oxide attenuation coefficient at 0.662 MeV was calculated using the XCOM (National Institute of Standards and Technology, U.S.A.) program. The theoretical attenuation coefficient of the lead oxide composites at 0.662 MeV was compared with the measured values in Figure3.7. The experimental values are in a sound agreement with the theoretical calculations. The

attenuation coefficient for the lead oxide composite sharply increased with the increasing of the weight fraction.

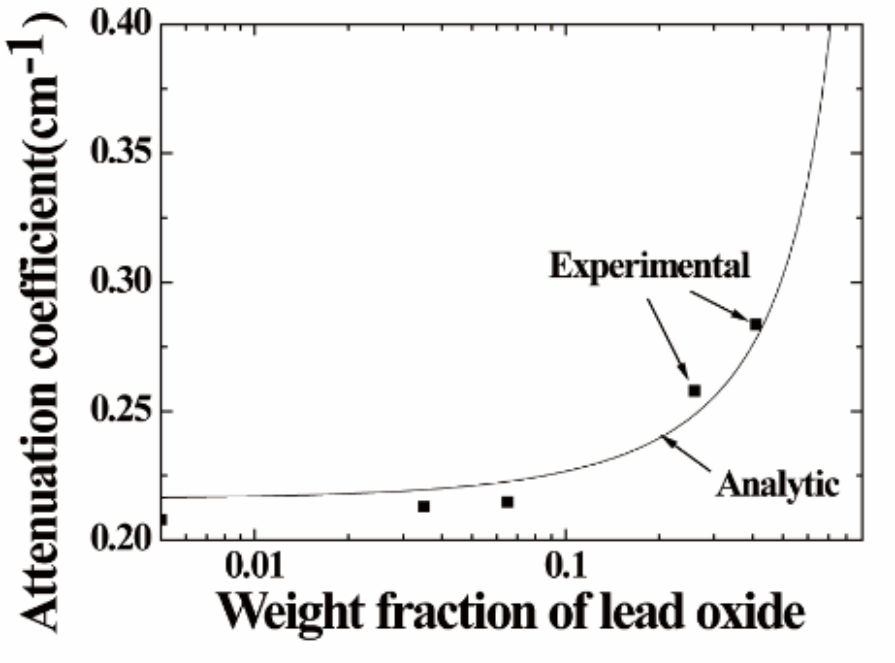

Figure 3.7. The calculated attenuation coefficient (solid line) and the comparison with the measurements (filled square data) for a lead oxide (PbO_2) composite.

3.3.4. The half-value layer

The half-value layer (HVL)—it was necessary to reduce the incident intensity of the γ-ray by half using the thickness of the radiation-shielding material—can be calculated using equation (1), as follows:

$$HVL = \frac{-ln0.5}{\mu}. \quad (4)$$

The effectiveness of the gamma-ray shielding is described in terms of the HVL of the PbO_2 composites, as shown in Figure 3.8. The lower the HVL value, the more effective the radiation material in terms of the thickness requirement. The increase of the PbO_2 content in the soft shield decreased the HVL.

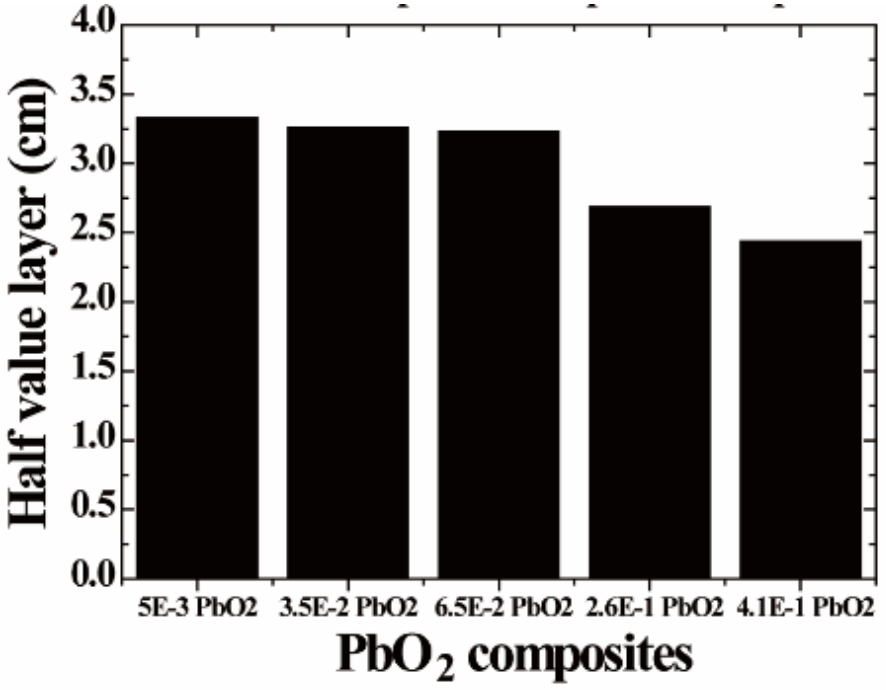

Figure 3.8. Variation of the half-value layer with the PbO_2 content in the soft shields.

3.3.5. Tensile test of the soft shields

Figures 3.9 show the tensile testing of the soft shield containing 3.33 M of lead oxide before and after the stretching up to 150 % strain, respectively.

The stress–strain curves of the soft shields with various metal-oxide concentrations are shown in Figures 3.10 (a), (b), and (c). Regarding the soft shield including iron oxide, the shape of the stress–strain curve is similar within small differences. It can be seen that as the amounts of the tungsten oxide and lead oxide particles was increased, the ductility of the soft shield was decreased. Figures 3.11 (a), (b), and (c) show the Young's modulus and the rupture strain of the soft shields with various shield-particle concentrations. As the soft shields contain particle quantities that are more than 3.33 M, the crosslink-formation of the soft shields becomes difficult due to the interaction between the crosslinking polymer and the metal-oxide particles. In the case of the soft shield containing iron oxide, the rupture strain is almost 1000 %, and only a slight change is evident regarding the concentration of the shielding particles. In addition, a slight increase of the Young's modulus was observed as the concentration of shielding particle was increased. However, for the soft shields containing WO_3 and lead oxide, the rupture strain decreased as the concentration of the shielding particle was increased. Alternatively, the Young's modulus was increased as the

concentration of the shielding particle was increased. It is expected that with a greater inclusion of the shielding particles, the soft shields will become more stiff but less stretchable.

The soft shields containing 0.33M of lead oxide were irradiated with γ-rays. In order to evaluate the stability of the soft shields to γ-ray, a tensile test was conducted before and after irradiation of the γ-ray. The γ-ray source was Cs-137 and the soft shields were irradiated for 4hours and 9hours. The stress-strain curves of the soft shields containing 0.33M of lead oxide are shown in Figure 3.12. The shape of the stress-strain curves before and after the γ-ray irradiation is similar. The Young's modulus and rupture strain before and after irradiation of the γ-ray shows little difference within the error range as shown in Figure 3.13. Therefore, the soft shields are stable in γ-rays.

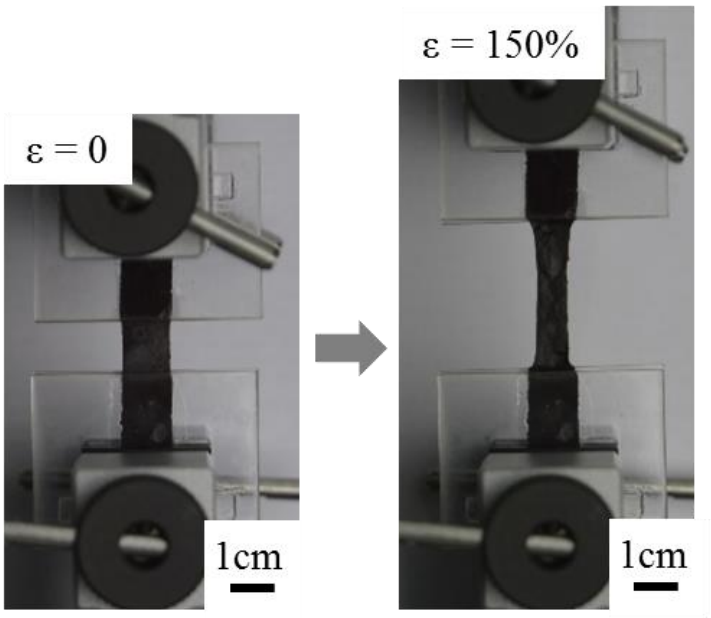

Figure 3.9. Tensile test of the soft shields containing 3.33 M of lead oxide (PbO_2) before and after stretching up to a 150 % strain, respectively.

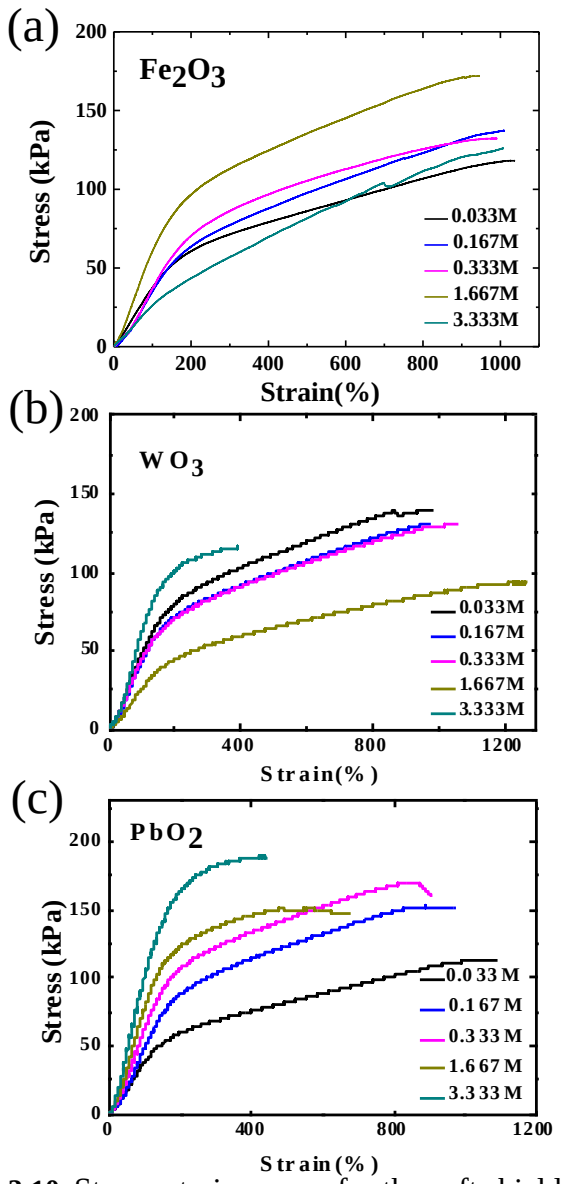

Figure 3.10. Stress–strain curves for the soft shields with various amounts of the shield particles until the mechanical fracturing of each sample.

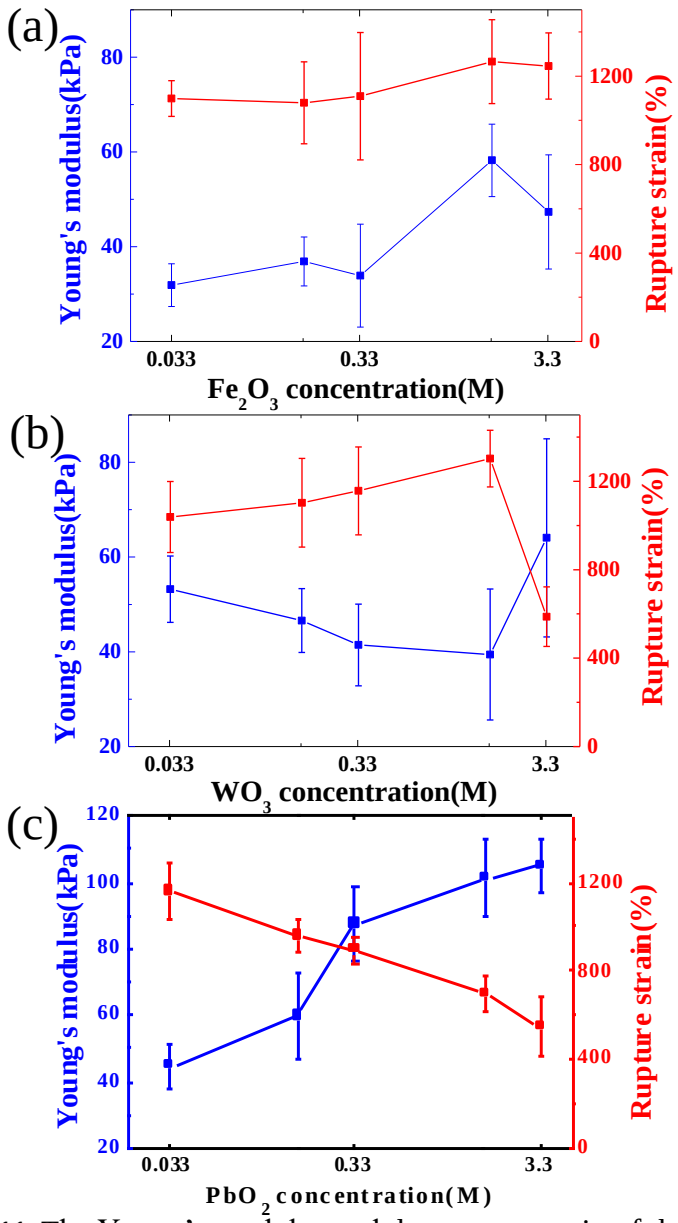

Figure 3.11. The Young's modulus and the rupture strain of the soft shields with various amounts of the shield particles.

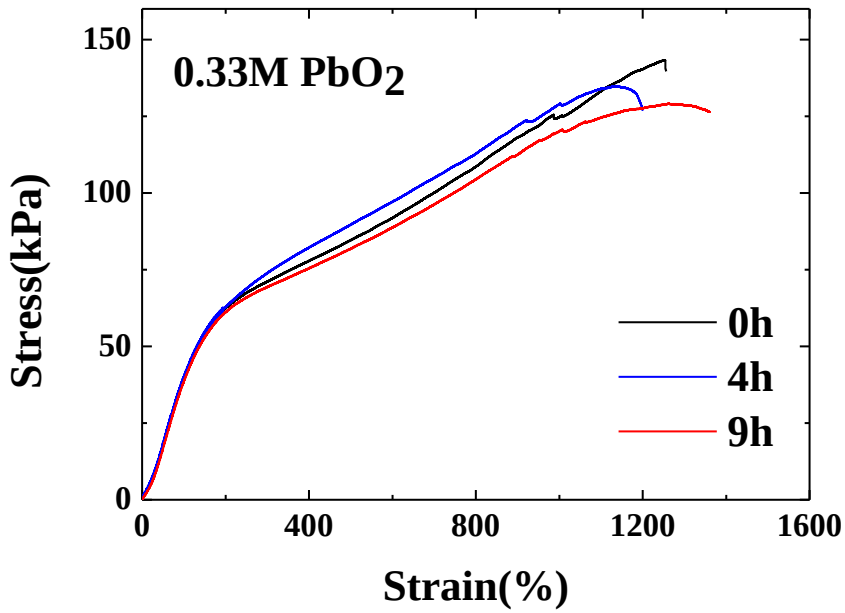

Figure 3.12. Stress-strain curves for the soft shields containing 0.33M of lead oxide with irradiated time.

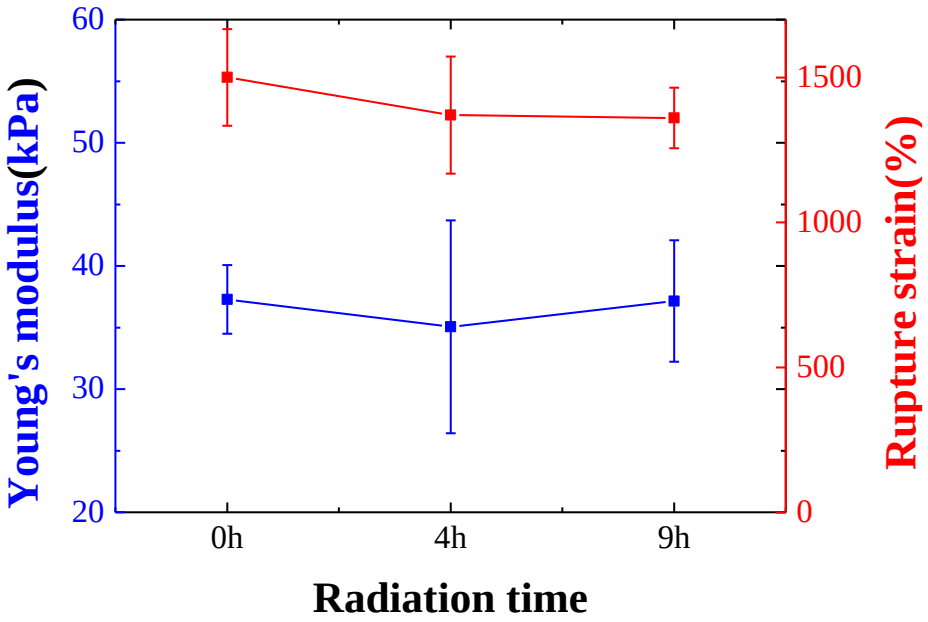

Figure 3.13. The Young's modulus and the rupture strain of the soft shield with irradiated γ-ray time.

3.3.6. Stitch test of the soft shields

The soft shields are soft but their mechanical toughness is sufficient for sewing. A stitch test was performed with the soft shield, as shown in Figures 3.14. The specimen size was adjusted to 10.0 × 25.0 × 3 mm^3, and a 100-μm silk-fiber diameter was sewed at the middle, 5 mm lower than the top surface, as shown in Figure 3.14. The stitch test for the sewed gel was performed with a loading rate of 6 mm/min. As shown in Figure 3.14, the stitched specimen was mounted on the tensile machine and then stretched until a mechanical rupture occurred from the stitching site.

A load-displacement curve of the stitched soft shields is shown in Figure3.15. A pristine soft shield was ruptured at the 128 mm displacement, but the soft shield containing 3.33 M lead oxide was ruptured at the 37 mm displacement. But interestingly, the soft shield containing lead oxide was able to withstand a load that is 1.5 times higher than that of the pristine soft shield by only one stitch. Due to the excellent energy dissipation in the soft shields from the interpenetration of the covalently crosslinked polyacrylamide with the ionically crosslinked alginate, a sewing may mean that the shield can withstand high stress concentrations.

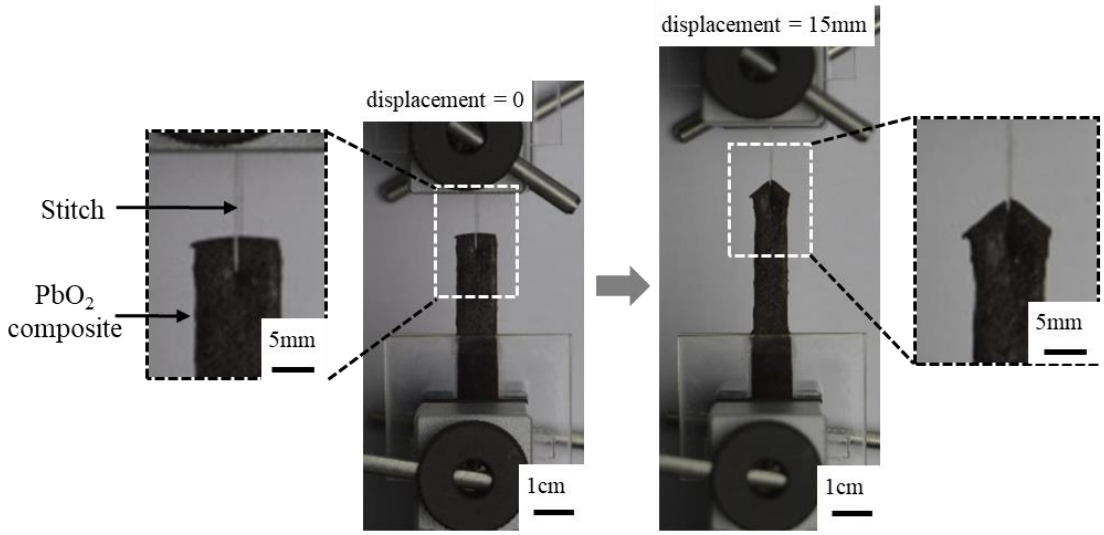

Figure 3.14. Stitch test of the soft shields containing 3.33 M of lead oxide (PbO_2).

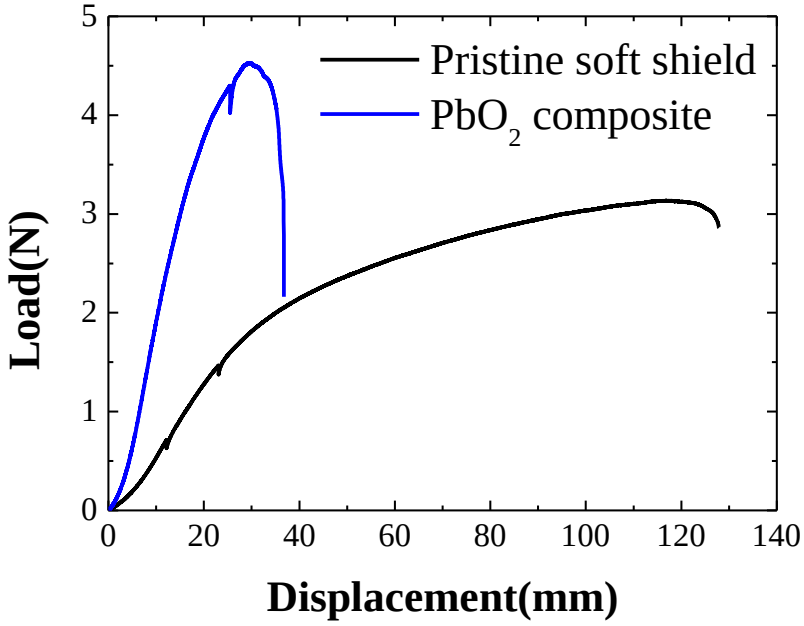

Figure 3.15. Load-displacement curves of the soft shields under stitch tests. A pristine soft shield and a soft shield with 3.33 M PbO_2 were examined.

3.3.7. Sewable soft shields

The soft shield was sewn several times, as shown in Figure 3.16 (a), and it was stretched with considerable power, as shown in Figure 3.16 (b); therefore, it is possible that they could provide resilience without the occurrence of a rupture. As shown in Figure 3.17, a wearable shield for the γ-ray radiation was simply made. The biocompatibility of the shield is expected to be high because the pristine hydrogel is biocompatible and the metal oxides that have been used in this work are nonreactive in a hydrogel matrix. Furthermore, it is expected that the shield will provide heat protection, since it contains a 51 wt% of water.

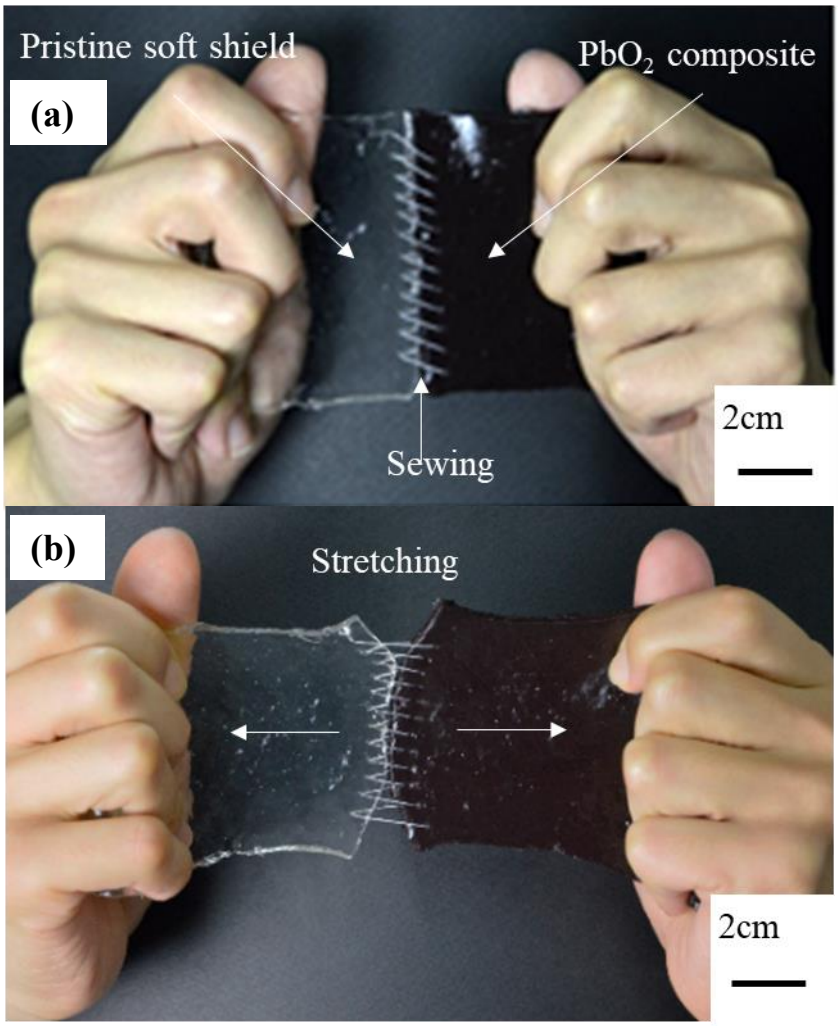

Figure 3.16. (a) - (b) A pristine soft shield was connected to a shield with PbO_2 by sewing. Both shields were kept intact after a stretching.

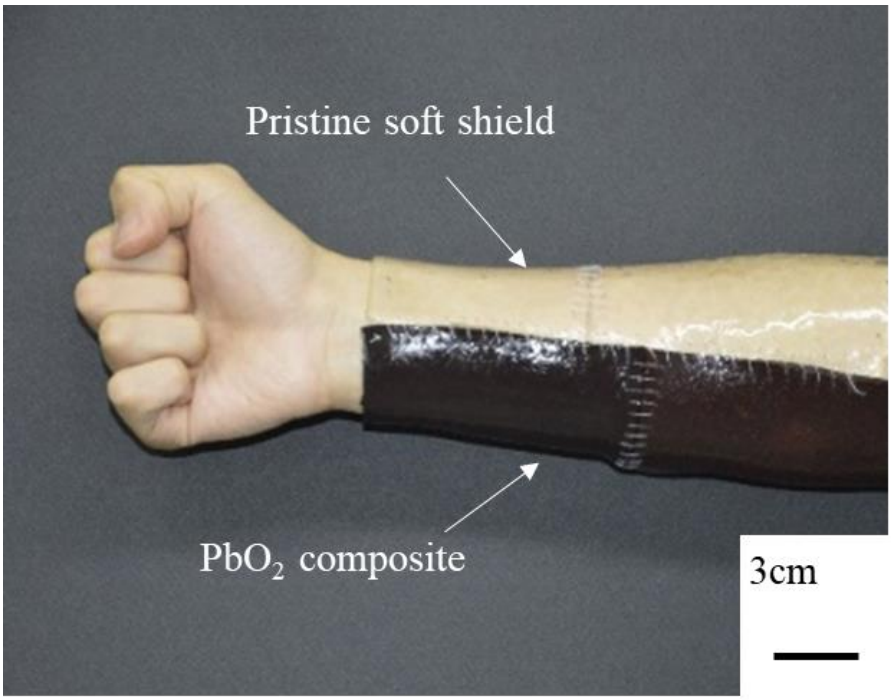

Figure 3.17. A wearable soft shield for the γ-ray radiation.

3.4. Conclusion

A sewable soft shield for radiation was synthesized through an integration of hydrogels and metal oxides. Sewable soft shields with a shielding ability and a wearability are applicable in areas of the nuclear industry such as transportation, the storage of radioactive materials, and the protection of the human body following a radioactive accident. In the case of the soft shields containing 3.33 M of Fe_2O_3, WO_3, and PbO_2, the attenuation coefficients are 0.229, 0.251, and 0.284 cm^{-1}, respectively, and they were stretched by more than 400 % without the formation of a rupture. The stretchability and energy-dispersion ability of the fabricated soft shield are high so that sewing can be performed. If the soft shield contains greater amounts of metal-oxide particles or higher-atomic-number metals, the attenuation coefficient of the soft shield can be increased because the probability of the interaction between the γ-ray and the electron is increased. The attenuation coefficient can be calculated with the amount of the contained shielding material using analytic calculations, so the control of the attenuation coefficient and the mechanical properties of the soft shield can be achieved by adjusting the contained material and contents. Accordingly, the soft shield can be used as a wearable shield in a radioactive environment, enabling researchers to form a more comprehensive

understanding of soft shields, thereby broadening the current soft-shield research and applications for radiation.

3.5. References

1. Brumfiel, G. Fukushima: Fallout of fear. Nature 493, 290-293 (2013).
2. Ten Hoeve, J. E. & Jacobson, M. Z. Worldwide health effects of the Fukushima Daiichi nuclear accident. Energy & Environmental Science 5, 8743-8757 (2012).
3. Siegbahn, K. Alpha-, beta-and gamma-ray spectroscopy. (Elsevier, 2012).
4. Bushberg, J. T. et al. Nuclear/radiological terrorism: emergency department management of radiation casualties. The Journal of emergency medicine 32, 71-85 (2007).
5. Nelson, G. & Reilly, D. Gamma-ray interactions with matter. Passive Nondestructive Analysis of Nuclear Materials, Los Alamos National Laboratory, NUREG/CR-5550, LAUR-90-732, 27-42 (1991).
6. Akkurt, I., Akyildirim, H., Mavi, B., Kilincarslan, S. &Basyigit, C. Gamma-ray shielding properties of concrete including barite at different energies. Progress in Nuclear Energy 52, 620-623 (2010).
7. Yılmaz, E. et al. Gamma ray and neutron shielding properties of some concrete materials. Annals of Nuclear Energy 38, 2204-2212 (2011).
8. Singh, K., Singh, N., Kaundal, R. & Singh, K. Gamma-ray shielding and structural properties of PbO–SiO 2 glasses. Nuclear Instruments

and Methods in Physics Research Section B: Beam Interactions with Materials and Atoms 266, 944-948 (2008).

9. Harrison, C. et al. Polyethylene/boron nitride composites for space radiation shielding. Journal of applied polymer science 109, 2529-2538 (2008).

10. Qin, F. &Brosseau, C. A review and analysis of microwave absorption in polymer composites filled with carbonaceous particles. Journal of applied physics 111, 061301 (2012).

11. Bartczak, Z., Argon, A., Cohen, R. & Weinberg, M. Toughness mechanism in semi-crystalline polymer blends: II. High-density polyethylene toughened with calcium carbonate filler particles. Polymer 40, 2347-2365 (1999).

12. Allaoui, A., Bai, S., Cheng, H.-M. & Bai, J. Mechanical and electrical properties of a MWNT/epoxy composite. Composites Science and Technology 62, 1993-1998 (2002).

13. Kim, C.-C., Lee, H.-H., Oh, K. H. & Sun, J.-Y. Highly stretchable, transparent ionic touch panel. Science 353, 682-687 (2016).

14. Keplinger, C. et al. Stretchable, transparent, ionic conductors. Science 341, 984-987 (2013).

15. Lee, Y. Y. et al. A Strain-Insensitive Stretchable Electronic Conductor: PEDOT: PSS/Acrylamide Organogels. Advanced Materials 28, 1636-

1643 (2016).

16. Annabi, N. et al. Highly Elastic and Conductive Human-Based Protein Hybrid Hydrogels. Advanced Materials 28, 40-49 (2016).

17. Calvert, P. Hydrogels for soft machines. Advanced materials 21, 743-756 (2009).

18. Lake, G. & Thomas, A. in Proceedings of the Royal Society of London A: Mathematical, Physical and Engineering Sciences. 108-119 (The Royal Society).

19. Gong, J. P., Katsuyama, Y., Kurokawa, T. &Osada, Y. Double-network hydrogels with extremely high mechanical strength. Advanced Materials 15, 1155-1158 (2003).

20. Haraguchi, K. &Takehisa, T. Nanocomposite hydrogels: a unique organic-inorganic network structure with extraordinary mechanical, optical, and swelling/de-swelling properties. Advanced Materials 14, 1120 (2002).

21. Ma, J. et al. Highly Stretchable and Notch-Insensitive Hydrogel Based on Polyacrylamide and Milk Protein. ACS Applied Materials & Interfaces 8, 29220-29226 (2016).

22. Sun, J.-Y. et al. Highly stretchable and tough hydrogels. Nature 489, 133-136 (2012).

23. Ehmann, W. D. & Vance, D. E. Radiochemistry and nuclear methods

of analysis. (1993).

24. Hubbell, J. Photon mass attenuation and energy-absorption coefficients. The International Journal of Applied Radiation and Isotopes 33, 1269-1290 (1982).

25. Hubbell, J. H. & Seltzer, S. M. Tables of X-ray mass attenuation coefficients and mass energy-absorption coefficients 1 keV to 20 MeV for elements Z= 1 to 92 and 48 additional substances of dosimetric interest. (National Inst. of Standards and Technology-PL, Gaithersburg, MD (United States). Ionizing Radiation Div., 1995).

요약 (국문 초록)

알지네이트는 다가의 양이온과 가교결합하여 하이드로젤을 형성할 수 있다. 알지네이트 젤은 결합 구조, 단량체의 성분, 고분자와 가교제의 농도에 따라 성질이 변화한다. 이중에서도, 이온 결합을 하는 알지네이트의 성질은 가교제로써 첨가되는 다가의 양이온에 따라 크게 영향을 받는다. 다가의 양이온에 의해 좌우되는 젤화 동역학에 대한 이해는 젤의 모듈러스, 평형상태에 도달하기 위패 필요한 시간, 젤의 회복 능력과 같은 다양한 성질을 조절하는 것을 가능케한다. 따라서 이온 결합을 하는 알지네이트의 젤화 동역학에 대해 연구해보았다. 양이온에 결합해있는 음이온의 종류에 따라 용해도에 차이가 있기 때문에 젤화되는 시간과 평형 상태에 도달했을 때의 점도가 변화하였다. 양이온이 같은 이온 가수를 가지더라도 주기가 커짐에 따라 평형 상태일 때 점도도 증가하였다. 알지네이트가 젤화 되는 동안 점도의 변화를 해석하기 위해 이론적인 모델 또한 연구하여 제시하였다.

다음장에서는 감마방사선을 차폐하기 위한 연성 차폐체가 연구되었다. 연성차폐체는 방사성 사고가 발생 시 인체를 보호하기

위한 용도 등으로 필요한 재료이다. 하지만 기존의 HDPE 와 에폭시 같은 재료는 모듈러스가 높아서 장갑이나 옷과 같은 입을 수 있는 형태로 제작하기 어려운 단점이 있다. 따라서 알지네이트 젤을 기반으로 신축성이 좋고 생체친화성이 좋은 연성차폐체를 제작하였다. 이 연성차폐체는 상호침투 결합을 하는 하이드로젤에 감마선 차폐 입자를 합성하여 제작되었다. 3.33 몰 농도의 PbO_2 입자를 포함하였을 때, 0.284 cm^{-1} 의 높은 차폐 계수를 가졌고, 파열없이 400% 길이까지도 늘어날 수 있었다. 게다가, 제작된 연성차폐체는 에너지 분산 능력이 높아서 직물 천의 보조 없이도 바느질로 꿰매질 수 있었다. 이러한 성질을 이용하여 합성된 연성차폐체를 직접 바느질하여 감마선을 차폐하면서 입을 수 있는 팔 토시도 제작해 볼 수 있었다.

위와 같은 본 연구를 통해 알지네이트의 젤화 동역학을 이해함으로써 다양한 재료로 이용될 수 있는 알지네이트의 물성을 조절할 수 있다. 그 예로 감마선을 차폐하는 연성 차폐체로의 응용도 가능함을 연구하였고 이 외에 다양한 재료의 기초 자료로 응용될 것으로 기대된다.

표제어 : 알지네이트, 젤화 동역학, 연성차폐체, 감마선 차폐, 입을 수 있는 차폐체

학 번 : 2011-20619